Local Density Augmentation in Supercritical Solvents: Electronic Shifts of Anthracene Derivatives

J. E. Lewis, R. Biswas, A. G. Robinson, and M. Maroncelli*

Department of Chemistry, 152 Davey Laboratory, The Pennsylvania State University, University Park, Pennsylvania 16802

Received: December 4, 2000; In Final Form: February 14, 2001

Fluorescence spectroscopy is used to measure local density augmentation in solutions of anthracene, 9-cyanoanthacene, 9,10-dichloroanthracene, and 9,10-diphenyl-anthracene in the supercritical solvents ethane, carbon dioxide, and fluoroform. For this purpose, the relationship between density and spectral shift is calibrated using dielectric continuum models of solvatochromism together with data in the gas phase and in liquid solutions. This approach, and the uncertainties inherent in it, are discussed in detail. The effective local densities (ρ_{eff}) deduced from the emission shifts in all of these solute/solvent combinations are comparable at temperatures near to the critical point (T_c +5 K or $T/T_c = 1.02$). Density enhancement factors ρ_{eff}/ρ increase with decreasing bulk density (ρ), reaching values of 5−6 at the lowest bulk densities observable. Density augmentation, the difference between the local and bulk densities ($\Delta\rho_{eff} \equiv \rho_{eff} - \rho$) reaches a maximum at densities of ~0.6 times the critical density (ρ_c). At this maximum, $\Delta\rho_{\text{eff}}/\rho_c$ takes on values between 0.6 and 1.0 in the different systems. Increasing the temperature leads to a substantial decrease in the density augmentation, but even 100 K above T_c, the effective local densities are still significantly larger than the bulk density. All of the effective densities observed, including this temperature dependence, can be reasonably correlated using single quantity, $\Delta G_{uv}/k_BT$: the ratio of the free energy of solute−solvent association, estimated using realistic potential models, and the thermal energy k_BT. These observations suggest that proximity to the critical point is probably only of secondary importance in determining the extent of density augmentation, at least on the very local scale probed by electronic spectral shifts.

I. Introduction

Local density augmentation, the greater-than-bulk solvent densities found near attractive solutes in supercritical solutions, is one of the unique features of solvation in supercritical fluids.[1−3] Evidence for such density augmentation comes from measurements of a host of different solute-centered quantities, such as partial molar volumes,[4] the friction on solute rotational and vibrational motion,[5−8] as well as a variety of spectroscopic observables.[3,9−11] Despite the obvious relevance of this phenomenon for modeling solubilities, diffusion rates, and reactivities of solutes in supercritical solvents, our quantitative understanding of local density augmentation in real systems is limited. Although theoretical approaches and computer simulations have provided a useful *qualitative* picture of the way in which attractive interactions give rise to density augmentation,[3,12] such studies have largely been confined to simplified model systems such as Lennard-Jones fluids. Direct comparisons to experiment have been rare.[13] On the experimental side, local densities have been measured in a wide variety of systems using a number of different techniques.[3] However, few systematic attempts have been made to *quantitatively* relate the local densities observed in experiment to characteristics of the solute−solvent interactions presumably responsible for augmentation.[14−16] We recently undertook such a comparison using new and previously published data from both computer simulation and experiment.[10] In that study, we showed that it is indeed possible to correlate the extent of local density augmentation in supercritical solutions to appropriate measures of the strength of solute−solvent interactions. We also noted that the extent of augmentation deduced from experimental studies is systematically larger than what is predicted by computer simulations. This discrepancy, whose origin has yet to be explained, highlights the fact that our current understanding of density augmentation in supercritical solvents is far from complete.

The present paper reports our recent efforts to add to the experimental database on local density augmentation. We have used steady-state emission spectroscopy to measure local densities in solutions consisting of a series of related solutes, anthracene, 9-cyanoanthracene, 9,10-dichloroanthracene, and 9,-10-diphenylanthracene, in the three supercritical solvents ethane, carbon dioxide, and fluoroform. These particular systems were chosen for two reasons. First, the electronic transition being observed in emission is similar in all of the solutes, being essentially the same $S_0 \leftrightarrow L_a$ transition found in the parent chromophore anthracene. This similarity, and the resolved structure of the anthracene spectrum are both advantageous for making accurate comparisons of spectral shifts and local densities in the different systems. Second, this series of solutes (and solvents) was chosen to provide a variable set of solute−solvent interaction types and strengths. Some molecular characteristics of the solutes and solvents investigated are summarized in Table 1. Note, for example, that 9-cyanoanthracene has a large dipole moment, 5 D, whereas all of the other solutes are nondipolar (but have significant quadrupole moments). Note also that 9,10-diphenylanthracene has approximately twice the volume, and thus total polarizability, of anthracene. The solvents too have distinctive characteristics. Despite the similarity of their

* Corresponding author. E-mail: mpm@chem.psu.edu.

10.1021/jp0043672 CCC: $20.00
Published on Web 03/31/2001

TABLE 1: Properties of the Solute and Solvent Molecules in this Study

species	T_c[a]/K	ρ_c[a]/mol dm^{-3-3}	P_c[a]/MPa	V[b]/Å^3	α[c]/Å^3	μ[c]/D	$\langle Q \rangle$[c]/DÅ
C_2H_6	305.4	6.74	4.88	45.4	3.3	0.0	0.9
CO_2	304.1	10.6	7.38	34.2	2.0	0.0	5.6
CHF_3	299.3	7.54	4.86	41.0	2.0	2.2	4.6
anthracene				166	22	0.0	19
9-cyanoanthracene				186	24	5.0	26
9,10-dichloroanthracene				195	25	0.0	23
9,10-diphenylanthracene				306	40	0.0	18

[a] Critical temperatures, densities, and pressures of solvents from Reid, R. C.; Prausnitz, J. M.; Poling, B. E. *The Properties of Gases and Liquids*, 4th ed.; McGraw-Hill: New York, 1987. [b] Molecular volumes estimated from van der Waals increments according to Edwards, J. T. *J. Chem. Ed.* **1970**, *47*, 261. [c] Polarizabilties, dipole moments, and effective axial quadrupole moments derived from ab initio calculations (at the MP2/6-31G* level for solvents and RHF/6-31G* level for solutes.) The effective quadrupole moments are provided as a measure of the importance of nondipolar electrical interactions as discussed in Reynolds, L.; Gardecki, J. A.; Frankland, S. J. V.; Horng, M. L.; Maroncelli, M. *J. Phys. Chem.* **1996**, *100*, 10337.

net self-interactions (as revealed by the similarity of their critical temperatures) C_2H_6 is a nonpolar molecule, CO_2 a quadrupolar molecule, and CHF_3 a dipolar molecule. Given these differences, we anticipated that the 12 solute−solvent pairs examined here would exhibit larger and hopefully understandable variations in density augmentation. Although the differences we determined at a fixed temperature were not as large as we had originally expected, the pattern of density augmentation found in the total data set, including temperature dependence, does appear to be understandable in terms of the strength of solute−solvent interactions relative to the thermal energy. The observations made here therefore support the conclusions made in the survey study by Song et al.[10] mentioned above. It should be noted that the lowest temperature data reported herein were already included in that earlier compilation. However, we have retaken much of the data on which the earlier values were based, revising some of the values accordingly, and have added temperature-dependent measurements not previously reported. The present work discusses the spectroscopy of these systems in more detail and also provides an analysis of the relationship between spectral shifts and local densities which we hope will be of general use.

II. Materials and Experimental Methods

The supercritical solvents C_2H_6 (99%), CO_2 (99.99%), and CHF_3 (99.995%) were purchased from Scott Specialty Gases and purified by passage through an oxygen trap (Oxisorb HP, MG Industries) prior to use. Liquid solvents (Aldrich) were either HPLC or spectrophotometric grade and were used without further purification. Solutes were obtained from Aldrich. Anthracene (99.9%) was used as received. 9-Cyanoanthracene ("9-CNA", 97%) was recrystallized twice from toluene and vacuum sublimed at 405 K. 9,10-Dichloroanthracene ("9,10-DClA", 98%) was recrystallized from ethanol solution followed by vacuum sublimation at 423 K. 9,10-Diphenylanthracene ("9,-10-DPhA", 97%) was recrystallized twice from acetic acid. All sublimations were performed in an argon atmosphere.

Spectroscopic measurements in supercritical solvents were made using stainless steel high pressure cells with quartz windows. The cells have an inner volume of approximately 10 cm^3 and an optical path length of 2 cm. Gases were introduced into the cells and maintained at a desired pressure using a syringe pump (Isco, model 100-DM) with an accuracy of ±1 psi. Data near room temperature (T<50 °C) were collected using cells that were temperature-regulated (±0.1 K) using a flow of thermostated water, either through the cell body, or with the cell immersed in the water (see below). For measurements at higher temperatures, a cell heated by two 250W cartridge heaters was employed. The temperature of this cell was regulated to ±0.5 K using a proportional controller (Omega Micromega CN77333). Samples were prepared by injecting an aliquot of stock solution into a cell and then driving off the carrier solvent with a stream of dry nitrogen gas. The concentration of the stock solution was chosen to produce a concentration of 2×10^{-6} M when the solute was completely dissolved. Data were typically collected at a fixed temperature for a series of increasing pressures. Usually a run would start at a relatively low pressure, and the pressure would be increased by successive additions of gas, thereby maintaining constant solute concentration. Between closely spaced pressure points the sample was equilibrated for at least 10 min while stirring with a magnetically coupled stir bar. After the highest pressure point the cell was vented (inevitably reducing the solute concentration) and refilled to the lowest pressure at which reasonable spectra could be obtained. A second series of increasing pressure points was then recorded with enough overlap with the first series to check for consistency. In most cases, several repeated runs were performed with a given solute/solvent/temperature combination and the results averaged in the final analysis.

Some comment is necessary concerning the effects of possible temperature and density heterogeneity of the supercritical samples used here. Fayer and co-workers[7] recently noted that local variations in temperature within spectroscopic cells can produce macroscopic density heterogeneities, which can be readily detected by observing the distortion of a laser beam passed through the supercritical sample. Using this method, we found that sample cells having unthermostated gas inlets above the spectroscopic viewing ports showed significant density inhomogeneities, presumably caused by the circulation of gas from the inlet tubing into the cell. In our cells the effect was noticeable over the whole compressible density range between 0.6 and 1.2 ρ_c and for temperatures as far as 10 K above T_c. Fayer and co-workers,[7] who reported similar behavior, found that these inhomogeneities could be eliminated by enclosing the entire spectroscopic cell and its input tubing in a temperature-regulated oven. They reported that only for temperatures within 2 K of T_c did the vibrational frequencies and lifetimes measured in this oven differ significantly compared to the results reported without this arrangement.[17]

To examine the effect of temperature/density inhomogeneities on the data collected in the present work, we measured spectra using two different methods of temperature regulation. The first was the method employed in our previous measurements near T_c.[5,18] In this case, water was circulated within the body of the supercritical cell to regulate the cell temperature, but apart from insulation, no attempt was made to regulate the temperature of the gas inlet tubing or valves. The second regulation scheme involved immersing the entire spectroscopic cell and its input

tubing and valves in circulating water contained within a plexiglass enclosure with quartz windows. Whereas macroscopic density inhomogeneities were clearly observable in the first arrangement, the immersion method rendered them unnoticeable for temperatures greater than 1 K above critical. Despite this clear difference in the apparent homogeneity of the samples, we could not detect any systematic differences between the spectra recorded using these two methods. For a number of solute/solvent combinations where direct comparisons were made, neither the frequencies nor the line widths/line shapes observed in the spectra differed significantly. For this reason, data from both of these cell arrangements (represented in roughly equal numbers of data sets) have been combined to obtain the results reported here.

Supercritical fluid densities were computed from measured values of temperature and pressure using the equations of state reported by Younglove and Ely for C_2H_6,[19] Ely et al. for CO_2,[20] and Rubio et al. for CHF_3.[21,22] Values of the refractive index (n) and dielectric constant (ϵ) parameters needed for solvatochromic analysis were determined using parametrizations as functions of density from literature sources.

For C_2H_6:[19,23,24]

$$\frac{n^2-1}{n^2+2} = 0.07741\rho_r + 1.097\times10^{-3}\rho_r^{\,2} - 5.427\times10^{-4}\rho_r^{\,3} \quad (1a)$$

$$\frac{\epsilon-1}{\epsilon+2} = [0.07660 + 4.334\times10^{-4}\ln(1+T_c/T)]\rho_r + 9.766\times10^{-4}\rho_r^{\,2} - 4.419\times10^{-4}\rho_r^{\,3} - 1.4568\times10^{-6}P \quad (1b)$$

For CO_2:[23−25]

$$\frac{n^2-1}{n^2+2} = 0.07016\rho_r + 1.412\times10^{-4}\rho_r^{\,2} - 3.171\times10^{-4}\rho_r^{\,3} \quad (2a)$$

$$\epsilon - 1 = 0.2386\rho_r + 0.02602\rho_r^{\,2} \quad (2b)$$

For CHF_3:

$$\frac{n^2-1}{n^2+2} = 0.05374\rho_r - 3.136\times10^{-4}\rho_r^{\,2} - 1.534\times10^{-4}\rho_r^{\,3} \quad (3a)$$

$$\frac{\epsilon-1}{\epsilon+2} = 0.1723\rho_r + 100.6\frac{\rho_r}{T}\exp(-0.1530\rho_r^{\,2}) \quad (3b)$$

where $\rho_r = \rho/\rho_c$ and the units of T and P are K and MPa, respectively. Equations 3a,b are the fits to primary data described in the Appendix.

For measurement of spectra in liquid solvents, a small amount of solute was dissolved in each liquid in a standard 1 cm fluorescence cuvette and diluted so as to have an absorbance of less than 0.1 at the S_1 absorption maximum. A solvent blank was also collected and subtracted from the spectrum of the solution during analysis. For gas-phase measurements, a T-shaped glass cell heated with Nichrome wire was used. A few crystals of the solute were loaded through a port on top of the cell, the cell was evacuated and then filled with N_2 to ensure thermal equilibration. The temperature of this cell was only regulated to ±3 K.

Fluorescence spectra were recorded using a SPEX Fluorolog F212 fluorometer with instrumental parameters chosen to provide a spectral resolution of 1 nm. In all cases the excitation wavelength was chosen to be near the maximum of the third resolved peak (in order of decreasing wavelength) of the absorption band. All spectra were corrected for spectral responsivity of the fluorometer and converted to a frequency representation prior to analysis.

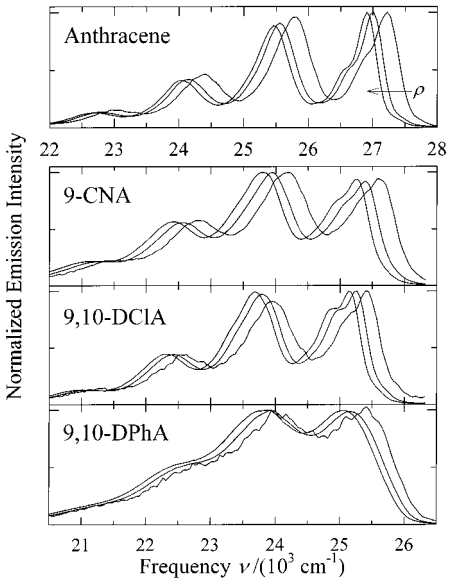

Figure 1. Representative fluorescence emission spectra of anthracene, 9-cyanoanthracene ("9-CNA"), 9,10-dichloroanthracene ("9,10-DClA"), and 9,10-diphenylanthracene ("9,10-DPhA") in supercritical C_2H_6 ($T_r \cong 1.02$) at three solvent densities. The densities shown are approximately 0.2, 1.0, and 2.0 ρ_c except for 9,10-DPhA, where the lowest density was 0.5 ρ_c. The arrow indicates the direction of the increasing solvent density.

The spectral frequencies reported here are those of the maximum of the *second vibronic peak of the emission spectrum* (in order of decreasing frequency). This peak was chosen instead of the more usual "0−0" peak in order to avoid possible errors due to self-absorption and Raman scattering, and to partially eliminate frequency changes resulting only from spectral broadening. The density dependence of this 2nd vibronic feature tracked that of the "0−0" band, but its frequency was found to be slightly more reproducible. The frequency was usually measured to a resolution higher than that at which the spectra were recorded by fitting the highest few (4−10) data points to an inverted parabola. At low densities, if spectra were noisy, frequencies were determined by comparing the spectrum in question to a reference spectrum recorded at high density and finding the frequency shift between the two using a least squares algorithm. This method allowed reproducible shifts (±50 cm^{-1}) to be determined even from relatively noisy spectra.

III. Electronic Spectra and the Determination of Local Densities

Representative emission spectra of anthracene, 9-cyanoanthracene ("9-CNA"), 9−10-dichloroanthracene ("9,10-DClA"), and 9,10-diphenylanthracene ("9,10-DPhA") in supercritical ethane are provided in Figure 1. These spectra are similar to the data for anthracene in supercritical solvents previously reported by several groups.[26−28] The shapes and widths of the spectra in supercritical media do not differ appreciably from those in liquid solvents of comparable polarity/polarizability. In both liquid and supercritical fluid solvents, the emission spectra of all of the solutes are similar in structure and bear a mirror image relationship to the corresponding absorption (or

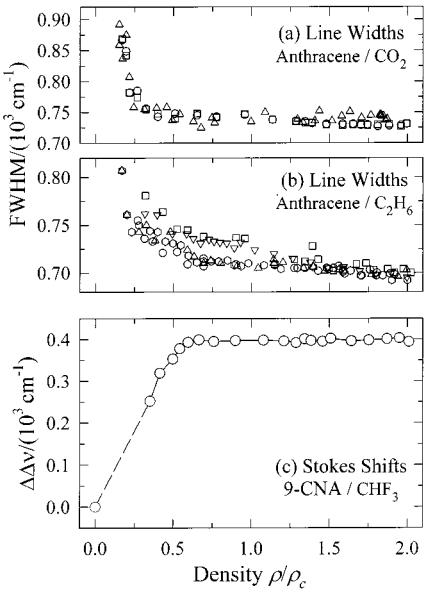

Figure 2. Examples of the changes in spectral widths and Stokes shifts observed as functions of solvent density ($T \cong 1.02\ T_c$). Parts a,b show values of the full widths at half maximum of the second vibronic feature of anthracene in CO_2 (three sets of data) and C_2H_6 (five sets of data). Uncertainties in these values are approximately ± 20 cm^{-1}. Part c shows the difference between the excitation and emission frequencies of 9-cyanoanthracene in CHF_3 (one data set) referenced to this same difference in the gas phase. The uncertainties in these differences are expected to be ± 70 cm^{-1}.

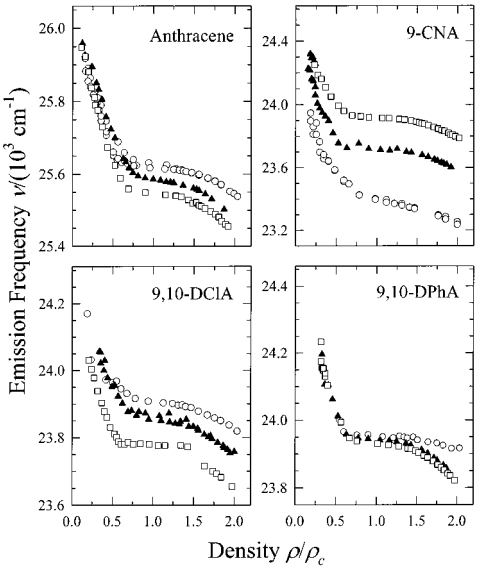

Figure 3. Representative density dependent frequency data observed with the various solute−supercritical solvent combinations studied here ($T/T_c \cong 1.02$). The frequencies correspond to the peak of the second vibronic feature in the emission spectrum. Squares, filled triangles, and circles denote data in C_2H_6, CO_2, and CHF_3, respectively. The gas-phase frequency of a given solute is positioned at the top left-hand corner of each panel.

excitation) spectra.[29] In all cases the primary change with solvent or solvent density is a frequency shift of the sort illustrated in Figure 1. Using such emission shifts to deduce local densities in supercritical solvents is the main focus of the present study. But before limiting our attention solely to these shifts, we digress to make a few comments concerning the line widths and Stokes shifts (the difference between excitation and emission frequencies) observed in these solute/supercritical solvent combinations.

Figure 2 illustrates the dependence of the line widths and Stokes shifts observed in select cases. Since the widths of the vibronic features in these spectra are primarily due to factors other than solvent broadening, the changes in line width with density are relatively modest. As illustrated in Figure 2(a,b), in anthracene, which has the most structured spectrum, the full width of the vibronic features increases by 15−20% from high to low densities over the accessible density range. Other solute/solvent combinations show less clear variations, but in no case is the effect pronounced. We note that there is nothing in these width variations that suggests that proximity to the critical density is of special importance. Rather, it appears that the observed width variations reflect an increasingly broad distribution in local environments as the density approaches the gas-phase limit.

The solvent-induced component of the Stokes shift (or solvent reorganization energy) is also of interest, in light of the surprising density dependence reported for this quantity in other systems. For example, in earlier work we found the Stokes shifts of coumarin 153 to be virtually independent of density (between 0.3 and $2.1\rho_c$) in several supercritical solvents,[18] while other workers reported that the Stokes shift of this polarity probe reaches a maximum at intermediate densities.[30,31] Neither result is expected: computer simulations predict a substantial decrease of the solvent reorganization energy with decreasing density.[32] Compared to coumarin 153, the solvent reorganization energies associated with the $S_0 \leftrightarrow S_1$ transition in all of the anthracene derivatives studied here should be small. In anthracene itself, the Stokes shift is less than 30 cm^{-1} in the liquid solvents we have examined. In supercritical CO_2, we could detect no Stokes shift greater than this value.[33] The other nondipolar solute/fluid combinations are likely to show comparably minute differences between absorption and emission shifts. The one exception we have measured[34] is the case of 9-cyanoanthracene in fluoroform, shown in Figure 2c. In this case, a density-independent solvent-induced Stokes shift of $\Delta\Delta\nu = 395 \pm 5$ cm^{-1} is observed over the density range $0.6 \leq \rho/\rho_c \leq 2.0$. Below $0.6\rho_c$ the solvent-induced component of the Stokes shift does show the expected drop toward the gas-phase value of zero, but as in the case of C153, the invariance of $\Delta\Delta\nu$ over a very broad density range is remarkable.

We now turn to the emission frequencies and their interpretation in terms of local solvent densities. Typical frequency/density data sets are displayed in Figure 3 for all 12 of the solute/supercritical solvent pairs ($T/T_c \cong 1.02$). The data are plotted such that the top left corner of each panel marks the gas-phase frequency. Squares, filled triangles, and circles denote data in ethane, CO_2, and fluoroform, respectively. These plots show that in these systems the shifts relative to the gas-phase lie within the range 450−1300 cm^{-1}, with the largest shifts being observed with the polar solute 9-cyanoanthracene. The frequencies in all three solvents appear to approach the gas-phase limits as density decreases, however, in dichloro- and diphenyl-anthracene roughly $^1/_3$ of the total shifts are not observed, due to the limited solubilities of these solutes at low solvent densities. Finally, we note that the sigmoidal shapes of all of these $\nu(\rho)$ data conform to the "3-density-regime" pattern most often observed in supercritical solvents.[11,35] The plateau region between $0.5 \leq \rho/\rho_c \leq 1.5$ apparently signals the presence of extensive density augmentation in these systems.

Determining local densities from such spectral data requires that one know the functional relationship between frequency and density. In the present study we adopt a dielectric continuum description of solvatochromism and assume that the shifts observed in supercritical fluids can be modeled in terms of the

TABLE 2: Emission Frequencies[a] in the Gas Phase and in Liquid Solvents

solvent	n_D[b]	ϵ_0[b]	anthracene	9-CNA	9,10-DClA	9,10-DPhA
gas phase	1	1	26.06	24.53	24.31	24.46
methanol	1.329	33.0	25.13	22.60	23.41	23.46
acetonitrile	1.342	35.9	25.02	22.70	23.32	23.33
diethyl ether	1.350	4.2	25.14	23.19	23.39	23.47
2-methylbutane	1.354	1.8	25.24	23.57	23.47	23.54
acetone	1.356	20.6	25.03	22.77	23.35	23.34
TCTFE[c]	1.356	2.4	25.17	23.39	23.44	23.45
methyl acetate	1.359	6.7	25.07	22.94	23.36	23.40
isopropyl ether	1.366	3.9	25.14	23.24	23.39	23.45
ethyl acetate	1.370	6.0	25.06	22.97	23.34	23.39
1-propanol	1.384	20.5	25.05	22.66	23.34	23.38
1-chlorobutane	1.400	7.4	25.01	23.03	23.27	23.30
tetrahydrofuran	1.405	7.6	24.95	22.86	23.22	23.27
propylene carbonate	1.420	64.9	24.89	22.54	23.17	23.19
cyclohexane	1.424	2.0	25.09	23.40	23.33	23.36
dimethylformamide	1.431	38.3	24.83	22.48	23.11	23.17
dimethylsulfoxide	1.478	46.5	24.67	22.29	22.98	23.06
1,2,4-trichlorobenzene	1.571	4.2	24.53	22.61	23.83	22.97

[a] The frequencies listed refer to the second highest frequency peak of the emission spectrum in units of 10^3 cm^{-1}. Spectral data in liquid solvents were recorded at room temperature (295 ± 2K), whereas the gas-phase frequencies were recorded at higher temperatures: 430 K, 390 K, 450 K and 520 K for the solutes anthracene, 9-CNA, 9,10-DClA, and 9,10-DPhA, respectively. The uncertainties in the frequencies are expected to be ±50 cm^{-1} in liquid solvents and ±100−150 cm^{-1} in the gas-phase spectra. [b] Refractive index and dielectric data (T = 298.2 K) are from Riddick, J. A.; Bunger, W. B.; Sakano, T. K. *Organic Solvents*, 4th ed.; Wiley: New York, 1986. [c] TCTFE = 1,1,2-trichlorotrifluoroethane.

TABLE 3: Constants Derived from Fits of Liquid-Solvent Frequencies to Equations 4 and 5[a]

solute	ν_0	α	β	standard error
anthracene	26.061	−3.870	−0.216	0.055
9-cyanoanthracene	24.532	−3.381	−1.251	0.029
9,10-dichloroanthracene	24.313	−3.903	−0.168	0.044
9,10-diphenylanthracene	24.460	−4.134	−0.227	0.029

[a] All values in units of 10^3 cm^{-1}.

variation of solvent dielectric properties with density. Specifically, we assume that the shift from the gas-phase frequency (ν_0) can be expressed in terms of the solvent refractive index n and dielectric constant ϵ by

$$\Delta\nu = \nu - \nu_0 = \alpha f(n^2) + \beta f(\epsilon) \tag{4}$$

where $f(x)$ is the reaction field factor

$$f(x) \equiv \frac{x-1}{x+2} \tag{5}$$

and α and β are constants characteristics of the solute. It should be noted that eqs 4 and 5 represent only one choice out of many possibilities for describing the relationship between dielectric parameters and spectral shifts.[36] This particular form is chosen because it is one of the simplest available, yet it is able to correlate the solvatochromic behavior of anthracene derivatives as accurately as other, more complicated forms. The solute-specific constants α and β in eq 4 are determined by fitting shifts observed in a series of liquid solvents, where the local and bulk dielectric properties are assumed to be identical.

Data used for calibrating the solvatochromic behavior of the four solutes are compiled in Table 2 and fit parameters (α and β) are summarized in Table 3. An example of one of these fits, for the solute 9-cyanoanthracene, is also provided in Figure 4. This figure, as well as the small standard errors listed in Table 3, indicate that eqs 4 and 5 accurately represent the solvatochromism of all of the solutes in liquid solvents. We note that the particular form chosen for the reaction field factor (eq 5) does impact the quality of the fits. If the other popular choice of reaction field factor

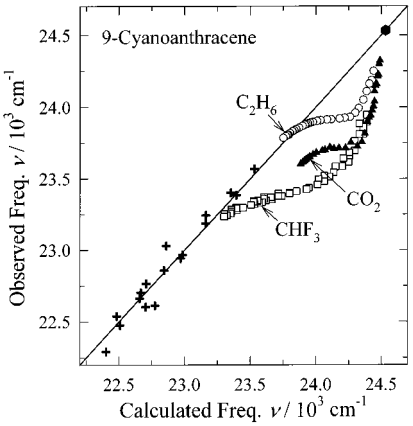

Figure 4. Example of the use of liquid−solvent and gas-phase data to calibrate the behavior of 9-cyanoanthracene. The "+" symbols and the highest-frequency point (hexagon) denote data in liquid solvents and in the gas-phase, respectively. The abscissa of this plot corresponds to frequencies calculated using eqs 4 and 5 with the factors α and β listed in Table 3. The remaining data were recorded in the supercritical solvents indicated at temperatures $T/T_c \cong 1.02$.

$$f'(x) = \frac{x-1}{2x+1} \tag{6}$$

is used in these correlations, the fit is poorer, with the standard errors being uniformly larger by about 50%, at least when the fit is constrained by use of the gas-phase frequency, as in eq 4.[37] The relative values of α and β in Table 3 indicate that the spectral shifts in all four solutes are primarily sensitive to the solvent's refractive index or its electronic polarizability $f(n^2)$ (measured by the coefficient (α + β)) rather than its nuclear polarizability $f(\epsilon) - f(n^2)$ (measured by β). Although there is a significant improvement in the fits for all solutes when the $f(\epsilon)$ term is included, only in the case of the dipolar solute 9-cyanoanthracene is the nuclear polarizability comparable in importance to the electronic term.

Once α and β are known for a given solute, the spectral shift expected at any density in a supercritical fluid can be calculated using the parametrizations of the density dependence of n and ϵ provided in the previous section. In all cases studied, the shifts so calculated can be conveniently expressed as quadratic

functions of density

$$\Delta\nu_{\mathrm{clc}}(\rho) = a_1\rho^1 + a_2\rho^2 \tag{7}$$

where the coefficients a_1 and a_2 depend on the identity of the solute and solvent (and to a slight extent on temperature in the case of 9-cyanoanthracene in CHF_3). The shifts calculated in this manner for 9-cyanoanthracene in supercritical solvents using bulk solvent densities are also shown in Figure 4. One finds that the observed shifts deviate from the correlation line by much more than the standard error of the fit (± 29 cm^{-1}), especially at intermediate densities. We interpret this deviation as indicating that the solute senses a local environment whose effective density differs substantially from the density of the bulk solvent used to predict the shifts.

Effective local densities can be inferred from data of the sort shown in Figure 4 in several ways. The most direct approach is to define effective densities by

$$\rho_{eff}' \equiv \rho(\Delta\nu_{\mathrm{obs}}) \tag{8}$$

where $\rho(\Delta\nu)$ is the functional inverse of $\Delta\nu_{\mathrm{clc}}(\rho)$. However, this approach is not optimal for two reasons. First, although eqs 4 and 5 describe the average behavior of liquid solvents rather well, small deviations from the average behavior are found in any given solvent. These deviations, which presumably result from differences in molecular size, shape, and charge distribution, not accounted for by the dielectric constants n and ϵ alone. It is best that these individual solvent variations not be directly translated into variations in effective densities. For example, in the data shown in Figure 4, the predicted shifts at high densities ($\rho_r \sim 2$, low ν) in ethane are slightly smaller than the observed shifts, whereas the predicted shifts in fluoroform are slightly larger. Direct application of eq 8 would therefore result in local densities slightly less than and slightly greater than the bulk density, respectively.[38] Given that the shifts in both cases (and in all cases except the CO_2 case shown in Figure 4) approach the correlation line to within the scatter of the liquid data, a more logical interpretation would be to assume that at high supercritical densities ($\rho_r \sim 2$) the local environment is comparable to one existing in a liquid solvent, i.e., is one that is "homogeneous" in density. The second reason for not interpreting eq 8 too literally is that in at least one case studied here, 9-cyanoanthracene in CO_2, also shown in Figure 4, the results are unreasonable. Direct application of eq 8 to the 9-cyanoanthracene/CO_2 system predicts local densities much greater than bulk densities over the entire density range. The reason for this erroneous prediction is that the dielectric constant of CO_2 does not adequately reflect the nuclear polarizability of this quadrupolar solvent.[39,40] Although the predictions for the other solutes are little affected by this error, because 9-cyanoanthracene is sensitive to the solvent nuclear polarizability, the 9-cyanoanthracene/CO_2 case cannot be reasonably represented in this fashion. Thus, if we want to treat all of the systems studied here on an equal footing, eq 8 cannot be used.

We therefore define local densities in a manner that allows for some "correction" of possible errors in the solvatochromic predictions for a given solvent/solute pair. Motivated by the observation that the supercritical data usually merge with the liquid solvent correlations at high densities, we choose a high-density reference point $\rho_{\mathrm{ref}} = 2\rho_{\mathrm{c}}$ where we require the effective local density to be equal to the bulk density. That is, we assume $\rho_{\mathrm{eff}} = \rho$ at $\rho = 2\rho_c$ in all systems, and define local densities relative to this fixed point. Given this definition, if the predicted spectral shifts are proportional to density, the particularly simple

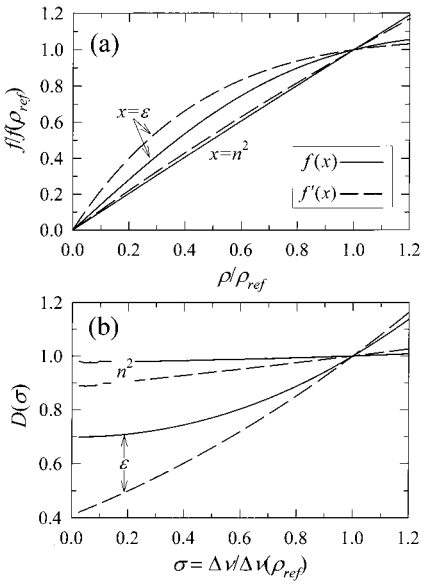

Figure 5. Illustration of the dielectric reaction field factors (a) and "distortion functions" (b) involved in translating between observed frequencies and effective local densities in CHF_3. In all cases the data have been normalized to unity at the reference density of $2\rho_c$ in order to display the relative departures from the simple relation $\rho_{\mathrm{eff}} \propto \Delta\nu_{\mathrm{obs}}$.

relationship

$$\rho_{\mathrm{eff}} = C\Delta\nu_{\mathrm{obs}} \qquad \text{where} \qquad C = \frac{\rho_{\mathrm{ref}}}{\Delta\nu_{\mathrm{obs}}(\rho_{\mathrm{ref}})} \tag{9}$$

is obtained. Partly as a result of our choice of the Clausius-Mossotti form for $f(x)$, in most of the systems studied here, eq 7 is closely approximated by $\Delta\nu_{\mathrm{clc}} \cong a_1\rho$, so that the effective densities are indeed expected to be proportional to the observed shifts. In such cases the measured shifts provide simple and direct indicators of effective local densities. In the more general case, the spectral shifts provide a "distorted" representation of the densities. In this spirit we consider reduced shifts, $\sigma(\rho) \equiv \Delta\nu(\rho)/\Delta\nu(\rho_{\mathrm{ref}})$, and define a "distortion function" by

$$D(\sigma) \equiv \frac{\rho_{\mathrm{clc}}(\sigma)}{\rho_{\mathrm{ref}}}\frac{1}{\sigma} \tag{10}$$

where $\rho_{\mathrm{clc}}(\sigma)$ is obtained from the relationship between the calculated frequency and density, i.e., from the inverse of $\sigma(\rho) \equiv \Delta\nu_{\mathrm{clc}}(\rho)/\Delta\nu_{\mathrm{clc}}(\rho_{\mathrm{ref}})$. Effective densities are then defined analogously to eq 9 by

$$\rho_{\mathrm{eff}} = D(\sigma_{\mathrm{obs}})\{C\Delta\nu_{\mathrm{obs}}\} = \rho_{\mathrm{clc}}(\sigma_{\mathrm{obs}}) \tag{11}$$

where $\sigma_{\mathrm{obs}} = \Delta\nu_{\mathrm{obs}}(\rho)/\Delta\nu_{\mathrm{obs}}(\rho_{\mathrm{ref}})$. This definition of ρ_{eff} utilizes the liquid solvatochromic data to determine the nonlinear form of the frequency-density mapping, through the use of $\rho_{\mathrm{clc}}(\sigma)$. However, in contrast to direct application of eq 8, it allows for some correction of possible errors in the solvatochromic predictions by virtue of the system-specific scaling factor C.

The distortion functions $D(\sigma)$ defined in this manner provide insight into the way in which local solvent densities are mapped onto a particular observable such as $\Delta\nu$. Figure 5 illustrates the components of this mapping in the most interesting case, fluoroform. The basic ingredients of the dielectric analysis are the reaction field functions $f(x)$ shown in Figure 5a. Here we compare the reaction fields $f(n^2)$ and $f(\epsilon)$ (eq 5, solid curves) and the alternative forms $f'(n^2)$ and $f'(\epsilon)$ defined by eq 6 (dashed

curves), all normalized to unity at $\rho_{ref} = 2\rho_c$. For either reaction field, the electronic polarizability of the solvent, represented by $x = n^2$ is approximately proportional to density. This near proportionality is also found in ethane and CO_2, and presumably in most other supercritical solvents as well. For spectral shifts dominated by electronic polarizability, dielectric models therefore predict $\Delta\nu_{clc} \cong a_1\rho$, as noted above. In contrast, the total polarizability $f(\epsilon)$ is far from a linear function of density in fluoroform. This nonlinearity results from the collective nature of the nuclear polarizability $f(\epsilon) - f(n^2)$, and it is absent in the nondipolar fluids ethane and CO_2, for which $\epsilon \cong n^2$. The reaction field function $f(\epsilon)$ is closer to a linear function than is its counterpart $f'(\epsilon)$, and when the nuclear solvent polarizability is an important determinant of the spectral shifts, these two reaction fields predict significantly different local densities, as will be shown explicitly later.

The distortion functions implied by these various reaction fields are illustrated in Figure 5b. These functions translate between observables such as $\Delta\nu$ and density in cases where one or the other dielectric property "n^2" or "ϵ" completely determines the behavior (i.e., when $\alpha = 0$ or $\beta = 0$ in eq 4). In general, the amount of "distortion" or deviation from a simple proportionality between frequency shift and density that is predicted for any given observable and solute depends on its relative sensitivity to the dielectric factors $f(n^2)$ and $f(\epsilon)$, i.e., on the ratio α/β. For the reaction field f used in this work, the net distortions, measured at $\rho = 0$ relative to $\rho = \rho_{ref}$, are relatively modest: ~20% in the case of 9-cyanoanthracene/fluoroform and ~10% for the remaining solute/solvent combinations. Use of the reaction field f' predicts roughly 2-fold greater distortion from the simple behavior $\Delta\nu_{clc} \propto \rho$. The consequences of the difference between f and f' will be examined further in the following section.

IV. Local Density Augmentation: Solute, Solvent, and Temperature Dependence

Representative examples of the effective densities derived from spectral shift data near to T_c ($T/T_c \cong 1.02$) are provided in Figures 6 and 7. Here and in the following figures, two quantities are used to display departure of the local density from that of the bulk solvent: the "density augmentation" $\Delta\rho_{eff} \equiv \rho_{eff} - \rho$ and the "density enhancement factor" ρ_{eff}/ρ. The data in Figure 6 are typical of what we observe in all of the solute−solvent combinations examined. Consistent with many previous studies,[3,10] we find that the density augmentation is maximal below the critical density. At the maximum in $\Delta\rho_{eff}(\rho)$, the effective local density is roughly 2.5 times the density of the bulk fluid. The enhancement factors (ρ_{eff}/ρ) are observed to increase monotonically from high to low densities, such that at the lowest densities measured, these enhancement factors reach values as large as 4−5.

The observation of a monotonic increase in ρ_{eff}/ρ with decreasing ρ differs from the behavior reported in some prior studies.[28,41−43] Since two of these studies involved similar emission shift measurements on some of the same systems studied here, it is worth pausing to consider their prior results. Rice et al.[43] reported values of ρ_{eff}/ρ for 9-cyanoanthracene at $T/T_c = 1.10$ in all three of the solvents studied here. In CO_2 they reported ρ_{eff}/ρ to have a sharp maximum as a function of ρ with a maximum value of ~2 at $0.6\rho_c$, which apparently decreases to ~1 at lower densities. In ethane they reported ρ_{eff}/ρ to have a broad maximum with a peak value of ~1.5 at $\rho \cong 0.9\rho_c$, which again appears to decrease to unity at lower densities. This behavior is unexpected, and quite different from what we report. Unfortunately, Rice et al. did not provide any primary data from which their effective densities were derived so that it is not possible to uncover the source of the disagreement. More recently, Zhang et al.[28] reported values of ρ_{eff}/ρ based on emission shifts of anthracene in CO_2 at 308 K. Their ρ_{eff}/ρ results also showed a maximum of ~1.7 at $0.5\rho_c$. In this case, the data were analyzed by fitting a line through the frequencies observed at the highest density points ($\rho \sim 1.8\rho_c$)

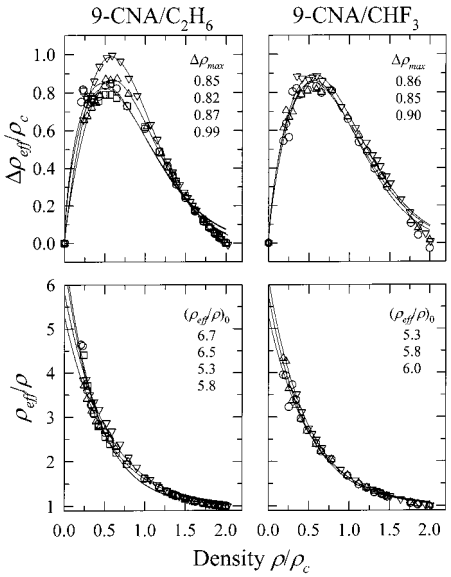

Figure 6. Representative effective density data for 9-cyanoanthracene in ethane and fluoroform ($T/T_c \cong 1.02$) calculated according to eq 11 (using the reaction field from eq 5). Effective densities are plotted in terms of the "density augmentation" $\Delta\rho = \rho_{eff} - \rho$ (top panels) and the "density enhancement factor" ρ_{eff}/ρ. The different symbols represent independent data sets, four in the case of ethane and three in the case of fluoroform. The solid curves are fits to eqs 12 and 13, which yield the values of $\Delta\rho_{max}$ and $(\rho_{eff}/\rho)_0$ indicated.

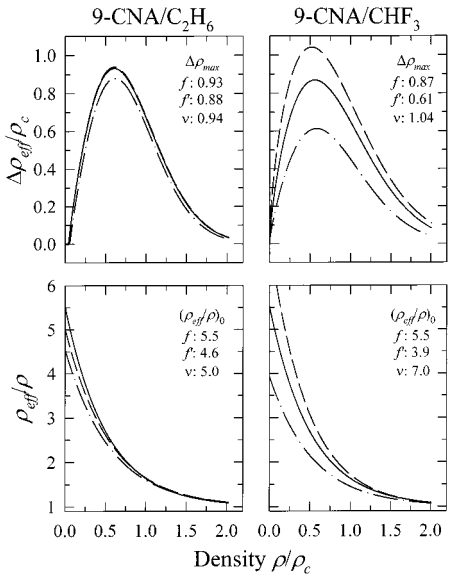

Figure 7. Illustration of the influence that different choices of the shift-density relationship have on the effective densities. Each curve represents a simultaneous fit of the composite of all repeated data sets in Figure 6. The solid curve is what is found when the frequency data is analyzed in the manner described in section III, i.e. using eq 11 and the reaction field $f(x)$ of eq 5. The dashed curves are results obtained using eq 9 (i.e., assuming $\rho_{eff} \propto \Delta\nu_{obs}$) and the dash-dot curves using eq 11 and the alternative reaction field factor $f'(x)$ defined in eq 6. Values of $\Delta\rho_{max}$ and $(\rho_{eff}/\rho)_0$ obtained from these analysis methods are indicated as "f", "ν", and "f'", respectively.

TABLE 4: Shifts and Augmentation Measures in Supercritical Fluids ($T/T_c \cong 1.02$)

solute/solvent		T/(K)	N^a	$\nu_0-\nu_{ref}$/cm^{-1}	$a_1{}^b$	$a_2{}^b$	$\delta\nu^c$/cm^{-1}	γ^c	$\rho_0{}^d/\rho_c$	$\Delta\rho_{max}{}^d/\rho_c$	$(\rho_{eff}/\rho)_0{}^d$
anthracene	C_2H_6	310	6	622	−0.325	0.004	+12	0.98	0.63	0.79 ± 0.14	3.9 ± 0.6
	CO_2	308	4	572	−0.294	0.000	−12	1.02	0.62	0.59 ± 0.10	2.3 ± 0.4
	CHF_3	305	2	515	−0.334	0.027	+41	0.93	0.63	0.91 ± 0.16	4.3 ± 0.7
9-CNA	C_2H_6	310	4	739	−0.394	0.044	+31	0.96	0.61	0.81 ± 0.14	4.9 ± 0.8
	CO_2	308	3	948	−0.344	0.040	−275	1.41	0.54	(0.9 ± 0.2)	(5 ± 1)
	CHF_3	306	3	1290	−0.903	0.140	−57	1.05	0.56	0.87 ± 0.15	5.5 ± 0.9
9,10-DClA	C_2H_6	310	3	613	−0.323	0.004	−48	1.03	0.61	0.92 ± 0.16	4.6 ± 0.8
	CO_2	308	2	554	−0.293	0.004	+15	0.97	0.63	0.84 ± 0.14	4.7 ± 0.8
	CHF_3	305	2	487	−0.308	0.022	+39	0.93	0.43	0.90 ± 0.15	4.8 ± 0.8
9,10-DPhA	C_2H_6	310	2	642	−0.346	0.004	+34	0.95	0.62	0.83± 0.14	4.4 ± 0.8
	CO_2	308	2	626	−0.314	0.004	−17	1.03	0.65	0.95 ± 0.16	4.5 ± 0.8
	CHF_3	305	2	548	−0.354	0.029	+42	0.93	0.67	1.03 ± 0.18	5.3 ± 0.9

[a] N is the number of independent experiments averaged in the final results. [b] a_1 and a_2 are the coefficients in the fit of $\delta\nu_{clc}(\rho)$, eq 7. [c] $\delta\nu$ is the difference between the observed and calculated frequencies at $\rho = \rho_{ref}$ and γ is the ratio of $(\nu_0 - \nu_{ref})$ determined from these observed and calculated reference frequencies. (See text.) [d] ρ_0 is the density at which $\Delta\rho_{eff}$ is maximal and $\Delta\rho_{max}$ is the maximum augmentation value. $(\rho_{eff}/\rho)_0$ is the density enhancement factor extrapolated to zero density. The estimated uncertainties listed here reflect both the uncertainties in the frequency determinations (including the value of ν_0) and, in the case of $(\rho_{eff}/\rho)_0$, uncertainties in extrapolation of the data to lower densities.

and using this line to determine ρ_{eff} at other densities. This method of analysis produces substantially negative values of ρ_{eff} at low densities and is not consistent with the methods employed here. However, that the frequency data tabulated by Zhang et al. is in reasonable agreement with our own. In fact, when their frequency data are reanalyzed using the present methods, the data yield augmentation values that are nearly identical to the ones we report. Thus, at least in this latter instance, the main source of the disagreement stems from use of alternative methods for extracting effective densities from the primary data. This example underscores the need for careful and consistent analysis if different solute−solvent systems are to be meaningfully compared.

Returning now to the discussion of the local density data, we summarize the information contained in plots like the ones shown in Figures 6 and 7 by fitting $\Delta\rho_{eff}(\rho)$ to a four-parameter "Weibull" function

$$\Delta\rho_{eff} = a\chi^{-\chi}e^{\chi}\left[\frac{\rho-\rho_0}{b}+\chi^{1/c}\right]^{c-1}\times \exp\left\{-\left[\frac{\rho-\rho_0}{b}+\chi^{1/c}\right]^{c}\right\}\chi=\frac{c-1}{c} \quad (12)$$

and ρ_{eff}/ρ data to the function

$$\rho_{eff}/\rho = 1 + a\exp(-b\rho) \quad (13)$$

The solid curves in Figure 6 are fits of this sort. Although these two functions lack theoretical justification, the fitted parameters $\Delta\rho_{max}$, the maximal value of the augmentation (a in eq 12), and $(\rho_{eff}/\rho)_0$, the extrapolated value of the enhancement factor at zero density ($1 + a$ in eq 13), provide convenient measures of the extent of augmentation in a given system. These two measures are complementary in the sense that they tend to emphasize the intermediate and low-density regimes, respectively.

Figure 6 contains augmentation data derived from analysis of several independent data sets recorded at the same temperature. The spread of these data reflect the frequency variability observed in the compressible regime ($0.5 \le \rho/\rho_c \le 1.5$). Although frequencies were found to be reproducible to better than ±20 cm^{-1} at high densities ($\sim 2\rho_c$), near to ρ_c frequencies were observed to vary by as much as 100 cm^{-1} in independent trials under ostensibly identical conditions.[44] This variability is one of the main sources of uncertainty in the determination of local densities. Values of $\Delta\rho_{max}$ and $(\rho_{eff}/\rho)_0$ derived from the different data sets (listed in Figure 6) were used to estimate uncertainties in the final augmentation results. Before discussing these results it is useful to consider an equally important source of uncertainty in the determination of local densities: the uncertainty associated with translating spectral shifts into densities.

Figure 7 illustrates the nature of this additional source of uncertainty, by displaying the results obtained from three slightly different methods of analyzing the data in Figure 6. Each of the curves shown here represents a simultaneous fit to all of the data collected in a given solvent. The solid curves ("f") are what is obtained when the method of analysis recommended in section II (eqs 11 and 5) is used. The dashed curves ("ν") result from simply assuming $\Delta\nu_{clc} \propto \rho$, i.e., by assuming that the distortion function in eq 10 is unity, and last, the dash−dot curves are obtained using the reaction field factor from eq 6 (f') rather than our preferred choice (eq 5, f). In the case of 9-cyanoanthracene in ethane, these various choices have little influence on the densities so obtained: all three methods yield results which differ by less than the scatter in the experimental data sets. The same holds true for all of the other solute−solvent combinations except 9-cyanoanthracene/fluoroform. In all but this latter system, the spectral shifts are mainly sensitive to the electronic polarizability of the solvent. In such a situation the distortion functions predicted by both dielectric continuum models are close to unity over the experimental data ranges. However, when the nuclear polarizability plays an important role, as in the case of 9-cyanoanthracene in fluoroform, the distortion functions differ significantly from unity and from one another (Figure 5). In this case the two methods of interpreting the observed frequencies lead to significantly different values of ρ_{eff}. The variations shown in Figure 7 for 9-cyanoanthracene/fluoroform serve as a reminder that the effective local densities determined here are subject to substantial uncertainties beyond those inherent in the experimental data. Conversion of the observed spectral shifts into densities relies on models of solvatochromism which are only approximate in homogeneous solutions, and their reliability in predicting the behavior in a heterogeneous environment is untested. The agreement observed among the various methods when electronic polarizability dominates, as in the 9-CNA/ethane data in Figure 7, is comforting. However, we note that such agreement still does not guarantee that the density dependence predicted by dielectric continuum models is accurate, even in these cases.

Having exposed the uncertainties inherent in translating spectral shifts into local densities, we now examine the results obtained according to the procedure recommended in section III. Tables 4 and 5 and Figures 6 and 8−10 summarize all of

TABLE 5: Temperature Dependence of Local Densities

system	T/K	T/T_c	$\nu_0-\nu_{ref}$/cm^{-1}	$\delta\nu^a$cm^{-1}	γ^a	$\rho_0{}^b/\rho_c$	$\Delta\rho_{max}{}^b/\rho_c$	$(\rho_{eff}/\rho)_0{}^b$
anthracene/C_2H_6	310	1.02	622	+12	0.98	0.63	0.79 ± 0.14	3.9 ± 0.6
	321	1.05	634	+07	0.99	0.68	0.62 ± 0.11	3.1 ± 0.5
	329	1.08	634	+04	0.99	0.62	0.48 ± 0.08	3.0 ± 0.5
	335	1.10	634	−13	1.02	0.62	0.54 ± 0.09	3.2 ± 0.5
	403	1.32	634	−66	1.10	0.63	0.35 ± 0.06	2.4 ± 0.4
anthracene/CO_2	308	1.03	572	−12	1.02	0.62	0.59 ± 0.10	2.3 ± 0.4
	324	1.06	559	−25	0.92	0.55	0.50 ± 0.10	2.1 ± 0.4
	357	1.18	560	−31	0.95	0.63	0.32 ± 0.05	1.7 ± 0.3
9-CNA/C_2H_6	310	1.02	739	+31	0.96	0.61	0.81 ± 0.14	4.9 ± 0.8
	335	1.10	841	−68	1.00	0.56	0.69 ± 0.12	4.4 ± 0.7
9-CNA/CO_2	308	1.01	948	−275	1.41	0.54	(0.9 ± 0.2)	(5 ± 1)
	357	1.12	722	−288	0.72	0.48	(0.5 ± 0.1)	(4 ± 1)
9,10-DPhA/C_2H_6	310	1.02	642	+34	0.95	0.62	0.83 ± 0.14	4.4 ± 0.8
	335	1.10	676	+41	0.94	0.61	0.56 ± 0.10	2.6 ± 0.4
9,10-DPhA/CO_2	308	1.01	626	−17	1.03	0.65	0.95 ± 0.16	4.5 ± 0.8
	357	1.18	610	+14	1.02	0.72	0.45 ± 0.08	2.2 ± 0.4

[a] $\delta\nu$ is the difference between the observed and calculated frequencies at $\rho = \rho_{ref}$, and γ is the ratio of $(\nu_0 - \nu_{ref})$ determined from these observed and calculated reference frequencies. [b] ρ_0 is the density at which $\Delta\rho_{eff}$ is maximal and $\Delta\rho_{max}$ is the maximum augmentation value. $(\rho_{eff}/\rho)_0$ is the density enhancement factor extrapolated to zero density. The estimated uncertainties listed here reflect both the uncertainties in the frequency determinations (including the value of ν_0) and, in the case of $(\rho_{eff}/\rho)_0$, uncertainties in extrapolation of the data to lower densities.

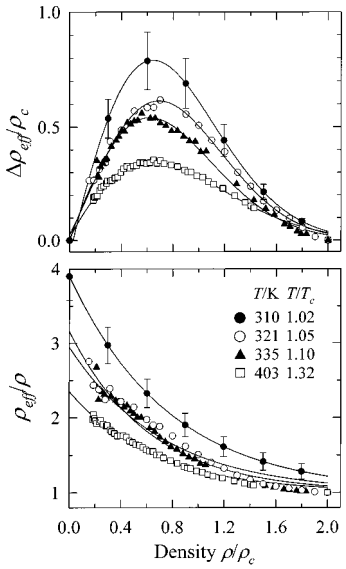

Figure 8. Effective density data for anthracene in C_2H_6 at four temperatures. The data points and error bars in the 310 K data represent the average and standard deviation observed in six independent sets of data recorded at this temperature. The remaining curves and points are individual data sets.

the information on effective local densities we have derived in this manner.

Table 4 contains data on all solute/solvent combinations at temperatures roughly 5 K above T_c ($T/T_c = 1.02$). The last three columns of this table list three characteristics measured from fits of data of the sort illustrated in Figure 6. ρ_0 is the density at which $\Delta\rho_{eff}$ is maximal, $\Delta\rho_{max}$ is the value of the augmentation at this maximum, and $(\rho_{eff}/\rho)_0$ is the value of the enhancement factor extrapolated to zero density. Although there are variations among the different solute/solvent combinations studied, more striking is the overall similarity in the effective densities exhibited by all of these systems. In all cases the density augmentation peaks at a density of $(0.61 \pm 0.11)\rho_c$ and, with only one exception, the maximal augmentation lies within the range $(0.8 - 1.0)\rho_c$. Similarly, in all but one case, values of $(\rho_{eff}/\rho)_0$ lie within ± 1 of the average value of 4.5. The exception to both of these statements is the anthracene/CO_2 system, which apparently exhibits significantly less density augmentation than the remaining systems. Apart from this outlier, the differences in $\Delta\rho_{max}$ and $(\rho_{eff}/\rho)_0$ among the different solute/solvent combinations, at least at $T/T_c = 1.02$, are close to the respective uncertainties in these characteristics.

Table 4 also summarizes a number of other quantities derived from the analysis described in section III. The entries labeled "$\delta\nu$" and "γ" are noteworthy in that they highlight the consistency of the present data and methods of analysis. Both quantities serve to indicate the extent to which use of eq 11 causes the observed densities to differ from those obtained via direct application of the liquid-state correlations (i.e., from eq 8). $\delta\nu$ is the difference between the observed and calculated frequencies at $\rho = \rho_{ref}$, and γ is the ratio of the reference shift $(\nu_0 - \nu_{ref})$ actually observed to the shift calculated using the liquid solvent calibrations (eq 4). The latter quantity is the factor by which the local densities that would have been computed using the liquid-phase correlations have been rescaled through use of the observed value of ν_{ref} in our analysis. From Table 4 one finds that in all but one case, $\delta\nu$ is comparable to the standard error in the liquid-solvent fits (Table 3) and the rescaling (γ) that is applied here amounts to a change of <10%. Thus, the methodology used to determine local densities seems sound. The one system for which there is a large discrepancy between observed and predicted behavior is 9-cyanoanthracene in CO_2. As discussed in the last section, this discrepancy is to be expected based on the quadrupolar nature of CO_2, and leads to substantial errors in dielectric predictions and thus in the results derived from direct application of eq 8. The present methodology, on the other hand, yields effective densities for this case which are in line with those found in the remaining systems. However, it is likely that these effective densities are slightly overestimated for the reason that the nuclear polarizability of CO_2, which is not accounted for here, should lead to a distortion function intermediate between the one used for CO_2 and that of fluoroform. Thus, the results for the 9-cyanoanthracene/CO_2 system are less certain and are listed in parentheses in Table 4.

Although the local densities determined here do not display any obvious trends with respect to solute and solvent variations at a single (reduced) temperature, they do depend systematically on temperature. Figure 8 illustrates the temperature dependence of $\Delta\rho_{eff}$ and (ρ_{eff}/ρ) observed in the case of anthracene in ethane. As illustrated in this figure, increasing the temperature leads to a decrease in the extent of the augmentation observed. It is noteworthy, however, that Figure 8 shows that substantial augmentation persists at temperatures far removed from the critical point. Even 100 K above T_c, although $\Delta\rho$ and (ρ_{eff}/ρ)

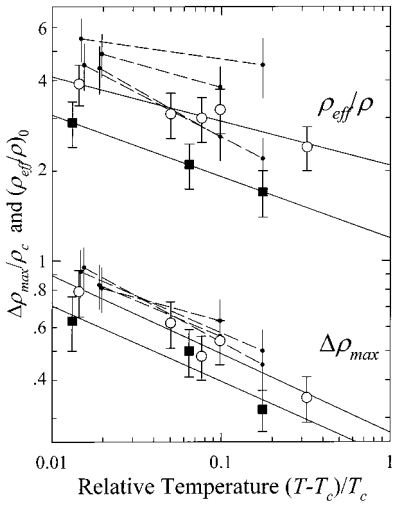

Figure 9. Summary of the temperature dependence of $\Delta\rho_{max}$ and $(\rho_{eff}/\rho)_0$ in a scaling-law format. The large open circles and large filled squares denote data in anthracene/C_2H_6 and anthracene/CO_2, respectively. The solid lines here are fits to the relationship $\Delta\rho_{max}$, $(\rho_{eff}/\rho)_0 \propto (1 - T/T_c)^p$. The pairs of smaller data points denote the remaining data on temperature dependence summarized in Table 5.

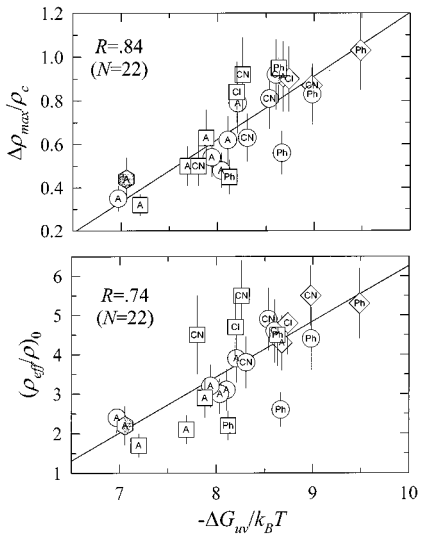

Figure 10. Correlation of $\Delta\rho_{max}$ and $(\rho_{eff}/\rho)_0$ with the free energy of association of isolated solute−solvent pairs, $\Delta G_{uv}/k_BT$, defined in eq 14. Data for all solute-solvent pairs at all temperatures are represented on this figure. Solutes are indicated by "A" = anthracene, "CN" = 9-cyanoanthracene, "Cl" = 9,10-dichloroanthracene, and "Ph" = 9,-10-diphenylanthracene, and solvents by (○) = C_2H_6, (□) = CO_2, and (◇) = CHF_3. The filled hexagon represents data for anthracene in methanol at 523 K, recorded by Bulgarevich et al.[45] *N* denotes the number of data points and *R* the correlation coefficient between the augmentation measures and $\Delta G_{uv}/k_BT$.

are reduced by about a factor of 2, the effective densities are still much higher than those of the bulk fluid. These observations appear to be general, as can be judged from the summary of temperature-dependent data provided in Table 5.

Given the persistence of augmented densities at temperatures far removed from T_c, one might question whether the phenomenon of augmentation is tied to the critical point at all. In an attempt to answer this question, in Figure 9 we plot $\Delta\rho_{max}$ and $(\rho_{eff}/\rho)_0$ as functions of temperature. To uncover any possible scaling behavior, a double logarithmic representation is used with temperatures plotted in terms of the variable $\tau \equiv (T - T_c)/T_c$. The two systems for which we have recorded data sets at more than two temperatures, anthracene/ethane (open circles) and anthracene/CO_2 (filled squares), exhibit similar behavior in this representation. In both systems, the maximum augmentation and the zero-density enhancement factor can be represented by a power-law, $A\tau^{-p}$, to within the uncertainties in the data. The exponent is found to be small in all cases, $0.15 \leq p \leq 0.26$. The remaining temperature pairs (small points connected by dashed lines) are also shown in Figure 9. With only two points, the temperature dependence in these latter systems is only crudely defined. Nevertheless, at least in the case of $\Delta\rho_{max}$, these data add to the impression that all of the data scale according to $\Delta\rho_{max} \propto \tau^{-p}$, with a single value of the exponent $p \sim 0.25$. It is not clear how much significance to attach to this apparent scaling behavior. In contrast to properties such as the partial molar volumes, which are directly tied to long-range correlations, the short-range properties $\Delta\rho_{max}$ and $(\rho_{eff}/\rho)_0$ cannot actually diverge as $T \rightarrow T_c$, so that fitting them in this manner may be inappropriate. We present Figure 9 merely to suggest that there may be some link, albeit a relatively weak one, between the extent of density augmentation and the divergence of many solvent properties as the critical point is approached.

Alternatively, proximity to the solvent's critical point might have little to do with the extent of density augmentation. Instead, the absolute temperature could simply affect augmentation by virtue of its appearance in some relevant Boltzmann factor. To test this idea we have examined the relationship between augmentation and various measures of the strength of solute−solvent interactions relative to the thermal energy k_BT. As discussed at length in a recent comprehensive study,[10] the association free energy ΔG_{uv} is one indicator of solute−solvent attraction capable of correlating the density augmentation observed in a wide range of simulated and experimental systems. This energy is defined by

$$\Delta G_{uv}/k_BT \equiv -\ln\{4\pi\int_0^{R_c} < \exp\{-u_{uv}(r,\bar{\Omega})/k_BT\} >_{\bar{\Omega}} r^2 dr\} \quad (14)$$

where u_{uv} is the solute−solvent pair potential, considered to be a function of the center-of-mass separation (r) and the relative orientation ($\bar{\Omega}$) of the solute and solvent. ΔG_{uv} values for the systems studied here were calculated with all-atom potentials of the Lennard-Jones plus Coulomb type, using parameters derived from a combination of ab initio calculations and transferable potential models. Details of the potentials and the calculations involved can be found in ref 10.

The measures of augmentation $\Delta\rho_{max}$ and $(\rho_{eff}/\rho)_0$ are plotted versus $\Delta G_{uv}/k_BT$ in Figure 10. Despite the considerable scatter, especially in the $(\rho_{eff}/\rho)_0$ data, it is clear that the single characteristic $\Delta G_{uv}/k_BT$ provides a reasonable guide to the relative extent of density augmentation for all of the solute−solvent combinations at all temperatures studied. It is noteworthy that the correlation shown in Figure 10 includes one point (⬢) from a previous measurement[45] of anthracene in supercritical methanol at 523 K − a fluid and temperature combination far removed from those measured here. The fact that $\Delta G_{uv}/k_BT$ apparently captures much of the variation in augmentation, while ignoring the location of the critical point, argues against the temperature effect being closely tied to solvent critical behavior. Rather, the results in Figure 10 suggest that increasing the temperature merely lessens the importance of the direct energetic factors affecting solute−solvent association, which appear to be the primary determinants of the local densities measured here.

V. Summary and Conclusions

In this work we have used emission shifts to measure effective local densities surrounding anthracene and three anthracene

derivatives in supercritical ethane, carbon dioxide, and fluoroform. To establish a relationship between emission frequency and local density, we first calibrated the sensitivity of each solute to the electronic and nuclear polarizability of its surroundings, using frequencies measured in the gas phase and in a series of liquid solvents. Such data in "homogeneous" environments can be accurately correlated using expressions derived from dielectric continuum models of solvatochromism. Assuming that the same correlations hold in the rarified environment of supercritical solvents, use of density-dependent dielectric data in supercritical solvents enables determination of the "local densities" sensed by the solute. We refer to such densities as "effective" because spectral shifts, or indeed any solute-centered observable, only defines a specifically weighted average of the density in some region surrounding the solute. The region of the solvent probed and the density weighting are characteristic of the particular property examined, such that different properties, for example spectral shifts,[3,10,11] partial molar volumes,[4] and radiative rates,[5] may provide very different perspectives on local density. In the case of emission shifts of the sort measured here, computer simulations[32] suggest that the effective densities being observed relate primarily to conditions within the first solvation shell of the solute.

A part of the present study consisted of assessing how sensitive the effective densities derived from solvatochromic shifts are to the details of the dielectric model (i.e., the particular reaction field) employed. When spectra are primarily sensitive to the electronic polarizability of the solvent, choice of dielectric representation has little influence over the densities obtained. In addition, the densities in this case are predicted to be nearly proportional to the observed shifts, which renders the translation between density and frequency particularly simple and direct. This is the limit into which nearly all of the solute−solvent combinations examined here fall. In contrast, when nuclear solvent polarizability is important, as in the case of 9-cyanoanthracene in fluoroform, the results depend significantly on details of the dielectric model employed, and the relationship between density and spectral shift is no longer a simple proportionality. For the 9-cyanoanthracene/fluoroform system, the density augmentation ($\Delta\rho_{max}$) derived from the spectral shifts varies by as much as 20−30% depending on which of two popular dielectric representations are used. This ambiguity serves as a reminder that the accuracy of any experimental determination of effective local densities is necessarily limited by the accuracy of the theoretical model relating the measured property to density. It should also be stressed again that the fact that different dielectric continuum models agree in situations where the electronic polarizability dominates is no guarantee that dielectric models are accurate even in these cases. In fact, we suspect that the discrepancy between the extent of density augmentation observed in experiments versus that found in computer simulations[10] may result, at least in part, from the inaccuracy of all continuum dielectric models in the low-density regime. The present data afford no new insights into this possibility, but it should be kept in mind that the magnitudes of the augmentation reported here (and in other studies) may be subject to further interpretation.

Assuming our dielectric modeling to be accurate, these effective densities provide a picture of the conditions prevailing in the first solvation shell of these solutes. Within a few degrees of the solvent's critical temperature ($T/T_c = 1.02$), the effective densities (ρ_{eff}) and their variation with bulk solvent density are similar in all of the solute−solvent combinations investigated. The density enhancement factors ρ_{eff}/ρ increase with decreasing bulk density (ρ), reaching limiting values we estimate to be 4.5 $\pm$ 0.8 as $\rho \rightarrow 0$. The density augmentation ($\Delta\rho_{eff} \equiv \rho_{eff} - \rho$) exhibits a maximum at densities of $(0.6 \pm 0.1)\rho_c$, rather than near the critical density itself, as has been noted in many prior studies of density augmentation.[3,10] In all but one of the systems (anthracene/CO_2) the value of $\Delta\rho_{eff}$ at its maximum lies within the range $(0.8-1.0)\rho_c$. This constancy was initially surprising to us. We had assumed that the range of solute and solvent characteristics spanned by these systems (Table 1) would provide substantial variations in the strength of solute−solvent interactions and thus lead to substantial variations in the local densities present under comparable conditions. However, detailed calculations of the sort performed in ref 10 show that, despite the differences in molecular characteristics, the net solute−solvent attraction (as measured by ΔG_{uv}) varies by less than 4 kJ/mol (1.6 k_BT) among the 12 solute−solvent pairs studied here. Apparently, such differences are not large enough to cause variations in the augmentation much larger than the uncertainties in the data.

One way to effect more significant variations in local densities is through temperature variation. Increasing the temperature from $T_c + 5$ K to $T_c + 50$ K decreases $\Delta\rho_{eff}$ by roughly a factor of 2. The observed temperature dependence can be fit to a power-law of the form $\Delta\rho_{max}$, $(\rho_{eff}/\rho)_0 \propto (1 - T/T_c)^p$, but the power is small ($p \sim 0.25$), such that even at 100 K above T_c the effective local density is still substantially larger than the bulk density. Moreover, we find that a single parameter, $\Delta G_{uv}/k_BT$, provides a reasonable guide to the relative extent of density augmentation found in all of the solute−solvent combinations at all of the temperatures studied. Since this parameter is ignorant of the location of the critical point, the present data appear to indicate that density augmentation has little to do with the critical behavior of the solvent. But it is probably too strong a statement to say that proximity to the solvent's critical point plays no role in density augmentation. Analysis of partial molar volume measurements have clearly established the fact that the excess density in a large spatial region surrounding the solute is directly tied to the divergence of density fluctuations as criticality is approached.[4,46,47] What the present results suggest is that the presence of this long-range density augmentation must have only a modest, secondary effect on the more local solvation properties probed by electronic spectroscopy.

Acknowledgment. The authors gratefully acknowledge financial support of this work by the National Science Foundation.

Appendix

Although two previous studies[48,49] have already developed parametrizations of the dielectric properties of CHF_3 in the near critical regime, neither was found to be completely satisfactory for the present application. We therefore collected literature data on the refractive index and dielectric constant of CHF_3 at temperatures near to T_c and refit these data as functions of reduced density and temperature.

Few refractive index measurements are available under the near-critical conditions of interest. The parametrization of eq 3a (which is for the refractive index at a wavelength of 514 nm) was derived from two reports of the low-density gas-phase behavior,[50,51] one value near the critical point,[52] and two points at liquid densities ($T = 173$ K, $\rho \sim 3\rho_c$)[53] by assuming that the molar refraction [$R_m \equiv (n^2 - 1)/(n^2 + 2)\rho$] is independent of temperature. Since the molar refraction varies by only $\pm$2% among all of these state points, eq 3a should be sufficiently accurate for most purposes.

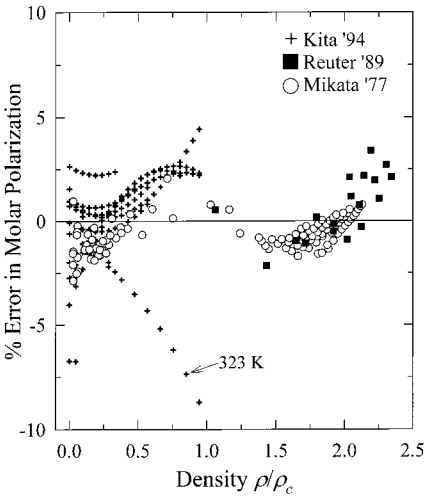

Figure 11. Summary of the deviations of the experimental molar polarizations measured by various authors (as indicated) and the polarization calculated according to eq A4.

The density and temperature dependence of the dielectric constant of fluoroform were fit using data from three primary sources. Mikata[54,55] measured ϵ at a series of 6 temperatures and 21 pressures surrounding the critical point. Reuter et al.[56] measured ϵ at nine temperatures and at a series of relatively high pressures ranging up to 2 kbar. Finally, Kita et al.[57] recently reported parametrizations of the molar polarization

$$P_{\mathrm{m}} = \left(\frac{\epsilon - 1}{\epsilon + 2}\right)\frac{1}{\rho} \tag{A1}$$

for densities below the critical density at a series of 10 temperatures between 273 and 353 K. Densities were computed from pressure/temperature data using the equation of state of Rubio et al.,[21,22] and all data were converted to a polarization representation, $P_{\mathrm{m}}(\rho,T)$, for fitting.

The functional form chosen to represent $P_m(\rho,T)$ was suggested by the observation that for a fixed temperature, Mikata's data (which provided the best density coverage) could be represented by a density dependence of the form

$$P_{\mathrm{m}} = a + b\exp(-c\rho_{\mathrm{r}}^{\,2}) \tag{A2}$$

The temperature dependence of P_{m} in the limit of zero density, as derived from the data of Kita[57] and others,[58,59] could be fit to a temperature dependence

$$P_m(\rho \to 0)/(10^{-6}\ \mathrm{m^3\,mol^{-1}}) = 6.403 + 1.775 \times 10^4\frac{1}{T} \tag{A3}$$

for temperatures $270 \le T \le 430$ K. On the basis of these observations, a least-squares fit was performed using all of the available data (represented as 276 points) spanning the temperature and density ranges $274 \le T \le 408$ K and $0 \le \rho/\rho_{\mathrm{c}} \le 2.3$ to the function

$$P_{\mathrm{m}}(\rho_{\mathrm{r}},T) = a + \frac{b}{T}\exp(-c\rho_{\mathrm{r}}^{\,2}) \tag{A4}$$

The best fit parameters were found to be $a = 2.281 \times 10^{-5}$ m^3 mol^{-1}, $b = 1.331 \times 10^{-2}$ m^3 mol^{-1} K, and $c = 0.1530$ with a standard error of fit of 1.0×10^{-6} m^3 mol^{-1}, or 1.8%. Deviations between the observed and calculated values of $P_{\mathrm{m}}(\rho_{\mathrm{r}},T)$ are shown in Figure 11. With few exceptions, such as the data labeled "323 K" whose density dependence appears different from the rest, the fit captures the density and temperature dependence of the observed data to better than ±3%. Thus, the parametrization provided in eq 3b (given simply by ρP_{m}) should provide an accurate representation of the dielectric constant of CHF_3 over the range $0.92 \le T/T_{\mathrm{c}} \le 1.36$ and $0 \le \rho/\rho_{\mathrm{c}} \le 2.3$.

The main differences between the dielectric behavior computed with eq 3b and those given by prior parametrization occurs at densities higher than ρ_{c}. The parametrization of Sun et al.[49] deviates markedly from eq 3b at high densities. It shows an essentially linear dependence of the reaction field factor $R \equiv (\epsilon - 1)/(\epsilon + 2)$ on density, such that for densities greater than $1.5\rho_{\mathrm{c}}$, R takes on unphysical values ($R > 1$). The parametrization of Rhodes et al.[48] differs from eq 3b primarily at densities greater than $1.5\rho_{\mathrm{c}}$. For $T \cong T_{\mathrm{c}}$ the Rhodes parametrization predicts that R and ϵ reach maximum values at $\sim 2\rho_{\mathrm{c}}$, whereas the present parametrization yields functions which continue to increase at least up to $2.5\rho_{\mathrm{c}}$. Some comparisons of the predictions of Rhodes et al. to those made using eq 3b for $T = T_{\mathrm{c}}$ are (Rhodes/eq 3b): at $\rho = 2.0\rho_{\mathrm{c}}$ $R = 0.67/0.71$ and $\epsilon = 7.0/8.4$, and at $\rho = 2.5\rho_{\mathrm{c}}$ $R = 0.59/0.76$ and $\epsilon = 5.4/10.2$. The behavior of eq 3b is expected to be more realistic at densities greater than $1.5\rho_{\mathrm{c}}$.

References and Notes

(1) For a number of reviews related to solvation in supercritical solvents, see: *Chem. Rev.* **1999**, *99*, issue 2. References 2 and 3 from this collection discuss the phenomenon of density augmentation extensively.
(2) Kajimoto, O. *Chem. Rev.* **1999**, *99*, 355.
(3) Tucker, S. C. *Chem. Rev.* **1999**, *99*, 391.
(4) Eckert, C. A.; Ziger, D. H.; Johnston, K. P.; Kim, S. *J. Phys. Chem.* **1986**, *90*, 2738.
(5) Heitz, M. P.; Maroncelli, M. *J. Phys. Chem. A* **1997**, *101*, 5852.
(6) Anderton, R. M.; Kauffman, J. F. *J. Phys. Chem.* **1995**, *99*, 13759.
(7) Myers, D. J.; Shigeiwa, M.; Fayer, M. D.; Cherayil, B. J. *J. Phys. Chem. B* **2000**, *104*, 2402.
(8) Schwarzer, D.; Troe, J.; Zerezke, M. *J. Chem. Phys.* **1997**, *107*, 8380.
(9) References 3, 10, and 11 summarize the results of many of the spectroscopic studies performed to date.
(10) Song, W.; Biswas, R.; Maroncelli, M. *J. Phys. Chem. A* **2000**, *104*, 6924.
(11) Sun, Y. P.; Bunker, C. E. *Ber. Bunsen-Ges. Phys. Chem.* **1995**, *99*, 976.
(12) Egorov, S. *J. Chem. Phys.* **2000**, *112*, 7138.
(13) A listing of the direct comparisons made between simulations and experimental data is provided in Table 7 of ref 10.
(14) Two recent studies in which a range of solutes were examined and density augmentation correlated to estimates of the relative strength of solute−solvent interactions are refs 15 and 16.
(15) Otomo, J.; Koda, S. *Chem. Phys.* **1999**, *242*, 241.
(16) Kanakubo, M.; Aizawa, T.; Kawakami, T.; Sato, O.; Ikushima, Y.; Hatakeda, K.; Saito, N. *J. Phys. Chem. B* **2000**, *104*, 2749.
(17) Urdahl, R. S.; Myers, D. J.; Rector, K. D.; Davis, P. H.; Cherayil, B. J.; Fayer, M. D. *J. Chem. Phys.* **1997**, *107*, 3747.
(18) Biswas, R.; Lewis, J.; Maroncelli, M. *Chem. Phys. Lett.* **1999**, *310*, 485.
(19) Younglove, B.; Ely, J. *J. Phys. Chem. Ref. Data* **1987**, *16*, 577.
(20) Ely, J.; Haynes, W.; Bain, B. *J. Chem. Thermodyn.* **1989**, *21*, 879.
(21) Rubio, R. G.; Zollweg, J. A.; Streett, W. B. *Ber. Bunsen-Ges. Phys. Chem.* **1989**, *93*, 791.
(22) Rubio, R. G.; Zollweg, J. A.; Palanco, J. M. G.; Calado, J. C. G.; Miller, J.; Streett, W. B. *J. Chem. Eng. Data* **1991**, *36*, 171.
(23) Besserer, G. J.; Robinson, D. B. *J. Chem. Eng. Data* **1973**, *18*, 137.
(24) For both of the nondipolar fluids ethane and CO_2 the distinction between ϵ and n^2 is negligible for our purposes, and these parametrizations, based on different types of data, yield values of the Clausius−Mossotti function $(x - 1)/(x + 2)$ which differ by no more than 3% in CO_2 and 1% in ethane over range of conditions relevant here.
(25) Moriyoshi, T.; Kita, T.; Uosaki, Y. *Ber. Bunsen-Ges. Phys. Chem.* **1993**, *97*, 589.
(26) Rice, J. K.; Niemeyer, E. D.; Bright, F. V. *Anal. Chem.* **1995**, *67*, 4354.
(27) Bunker, C. E.; Rollins, H. W.; Gord, J. R.; Sun, Y. P. *J. Org. Chem.* **1997**, *62*, 7324.
(28) Zhang, J.; Roek, D. P.; Chateauneuf, J. E.; Brennecke, J. F. *J. Am. Chem. Soc.* **1997**, *119*, 9980.

(29) The main exception to this statement is that in 9,10-diphenylanthracene the widths of the vibronic features are much broader in emission than in absorption, presumably to differences in the phenyl torsional potential in the S_0 and S_1 states.

(30) Takahashi, K.; Fujii, K.; Saeamura, S.; Jonah, C. *Radiat. Phys. Chem.* **1999**.

(31) Kimura, Y.; Hirota, N. *J. Chem. Phys.* **1999**, *111*, 5474.

(32) Patel, N.; Frankland, S. J. V.; Maroncelli, M. Computer Simulations of Supercritical Solvation: Coumarin 153 in CO_2 and Ethane. Manuscript in preparation.

(33) Brennecke and co-workers[28] also recently measured the absorption and emission shifts of anthracene in CO_2, and their data lead to the same conclusion.

(34) We would also expect a measurable Stokes shift for 9-cyanoanthracene in CO_2, and possibly also in ethane, but we have recorded excitation spectra in these systems.

(35) Sun, Y.-P.; Fox, M. A.; Johnston, K. P. *J. Am. Chem. Soc.* **1992**, *114*, 1187.

(36) Koutek, B. *Collect. Czech. Chem. Commun.* **1978**, *43*, 2368.

(37) The main difference lies in the inability of the latter reaction field to simultaneously account for both the liquid solvent and the gas-phase data. When ν_0 is allowed to vary freely, both reaction fields fit the liquid-solvent data equally well. However, in this case use of $f(x)$ yields values of ν_0 that are an average of 250 cm^{-1} high of the gas-phase value whereas $f'(x)$ yields values that are too high by an average of 700 cm^{-1}. Renge[60] has previously noted a similarly improved agreement with gas-phase data when the reaction field in eq 5 is used in favor of that in eq 6.

(38) It should be kept in mind that in a dense liquid, either at the densities of $\rho_r \sim 2$ easily achieved in supercritical solvents or at the densities ($\rho_r \sim 2.75$) typical of liquid solvents, the true density in the first solvation shell of most solutes is in fact larger than the bulk solvent density due to packing effects. The effective local densities determined here are only measured relative to the local density present in a typical liquid situation, which is defined to be the "bulk" density.

(39) Reynolds, L.; Gardecki, J. A.; Frankland, S. J. V.; Horng, M. L.; Maroncelli, M. *J. Phys. Chem.* **1996**, *100*, 10337.

(40) Khajehpour, M.; Kauffman, J. *J. Phys. Chem. A* **2000**, *104*, 9512.

(41) Carlier, C.; Randolph, T. W. *AIChE Journal* **1993**, *39*, 876.

(42) Zhang, J.; Lee, L. L.; Brennecke, J. F. *J. Phys. Chem.* **1995**, *99*, 9268.

(43) Rice, J. K.; Niemeyer, E. D.; Bright, F. V. *J. Phys. Chem.* **1996**, *100*, 8499.

(44) The widths of spectral features also varied in the compressible regime, as illustrated by the multiple sets of anthracene/ethane data shown in Figure 2b. We noted a modest correlation between the measured widths and frequencies in multiple data sets wherein narrower line widths were correlated with lower frequencies (greater augmentation). Although the presence of such a correlation suggests that some uncontrolled factor influences the data in the compressible regime, we were unable to discover what this factor might be. It does not appear to be related to the presence or absence of the macroscopic temperature/density inhomogeneities discussed in section II.

(45) Bulgarevich, D.; Sako, T.; Sugeta, T.; Otake, K.; Takebayashi, Y.; Kamizawa, C.; Uesugi, J.; Kato, M. *J. Chem. Phys.* **1999**, *111*, 4239.

(46) Debenedetti, P. G.; Mohamed, R. S. *J. Chem. Phys.* **1989**, *90*, 4528.

(47) Chialvo, A. A.; Cummings, P. T. *AIChE Journal* **1994**, *40*, 1558.

(48) Rhodes, T. A.; O'Shea, K.; Bennett, G.; Johnston, K. P.; Fox, M. A. *J. Phys. Chem.* **1995**, *99*, 9903.

(49) Sun, Y. P.; Bennett, G.; Johnston, K. P.; Fox, M. A. *J. Phys. Chem.* **1992**, *96*, 10001.

(50) Buckingham, A.; Graham, C. *Proc. R. Soc. (London)* **1974**, *A336*, 275.

(51) Burns, R.; Graham, C.; Weller, A. R. M. *Mol. Phys.* **1986**, *59*, 41.

(52) Yata, J.; Hori, M.; Kawakutsu, H.; Minayama, T. *Int. J. Thermophys.* **1996**, *17*, 65.

(53) Yoshihara, A.; Anderson, A.; Aziz, R.; Lim, C. *Chem. Phys.* **1981**, *61*, 1.

(54) Mikata, T.; Kubota, H.; Tanaka, Y.; Kashiwagi. *Refrigeration* **1977**, *52*, 543.

(55) Downing, R. *Fluorocarbon Refrigerants Handbook*; Prentice Hall: Englewood Cliffs, 1988.

(56) Reuter, K.; Rosenzweig, S.; Franck, E. U. *Phys. A* **1989**, *156*, 294.

(57) Kita, T.; Uosaki, Y.; Moriyoshi, T. Static Relative Permittivity of some Compressed Fluids. In *High-Pressure Liquids and Solutions*; Taniguchi, Y., Senoo, M.,Hara, K., Eds.; Elsevier: New York, 1994; p 181.

(58) Sutter, H.; Cole, R. *J. Chem. Phys.* **1980**, *52*, 132.

(59) Buckingham, A.; Raab, R. *J. Chem. Soc.* **1961**, *57*, 5511.

(60) Renge, I. *J. Photochem. Photobiol. A* **1992**, *69*, 135.